High-performance MoS_2/Si heterojunctions broadband photodetectors from deep UV to NIR

ZHENHUA LOU,[1] LONGHUI ZENG,[2] YUANGE WANG,[1] DI WU,[1,*] TINGTING XU,[1] ZHIFENG SHI,[1] YONGTAO TIAN,[1] XINJIAN LI,[1] AND YUEN HONG TSANG[2,*]

[1]*Department of Physics and Engineering, and Key Laboratory of Material Physics, Zhengzhou University, Zhengzhou, Henan, 450052, P.R. China*
[2]*Department of Applied Physics and Materials Research Center, The Hong Kong Polytechnic University, Hung Hom, Kowloon, Hong Kong, China*
**Corresponding author: wudi1205@zzu.edu.cn, yuen.tsang@polyu.edu.hk*

Received XX Month XXXX; revised XX Month, XXXX; accepted XX Month XXXX; posted XX Month XXXX (Doc. ID XXXXX); published XX Month XXXX

Polycrystalline 2D Layered molybdenum disulfide (MoS_2) films were synthesized *via* a thermal decomposition method. The MoS_2/Si heterostructures were constructed *in situ* by synthesis MoS_2 on plane Si substrates. Such MoS_2/Si heterostructures exhibited high sensitivity to light illumination with wavelengths ranged from the deep ultraviolet to the near-infrared. Photoresponse analysis reveals that a high responsivity of 23.1 A/W, a specific detectivity of 1.63×10^{12} Jones and a fast response speed of 21.6/65.5 μs were achieved. Notably, the MoS_2/Si heterojunction photodetector could operate with excellent stability and repeatability over a wide frequency range up to 150 kHz. The high performance could be attributed to the high-quality heterojunction between MoS_2 and Si obtained by *in situ* fabrication process. Such high performances with broadband response suggest that MoS_2/Si heterostructures could have great potential for optoelectronic applications. © 2015 Optical Society of America

OCIS codes: *(140.3490) Lasers, distributed-feedback; (060.2420) Fibers, polarization-maintaining; (060.3735) Fiber Bragg gratings; (060.2370) Fiber optics sensors.*

http://dx.doi.org/10.1364/OL.99.099999

In recent years, a great research effort has been devoted to explore the two-dimensional (2D) layered semiconductors nanostructures for new electronic and optoelectronic applications based on their specific geometries and distinct properties [1-4]. Among these 2D nano-materials, molybdenum disulfide (MoS_2) is one of the most studied layered materials due to its inherent and layer-dependent band-gaps [5-8]. By reducing layer number, the MoS_2's band-gap will change from 1.2 eV (indirect-gap) to 1.9 eV (direct-gap). Therefore, MoS_2 have been used for fabricating the electronic devices with high On/Off ratio and low power consumption [9-11]. Moreover, multilayer MoS_2 can offer a wider spectral response than single-layer MoS_2 from ultraviolet (UV) to near infrared (NIR) wavelengths due to its narrower band-gap, which is advantageous to various of photodetector (PD) applications. These unique and favorable features of MoS_2 have also made it an excellent candidate for developing high-performance and multifunctional electronic and optoelectronic devices, especially for photodetectors [12-14].

Recently, many researches concentrated on studying and improving device performances of MoS_2-based PDs. For example, Zhang et al. demonstrated the first monolayer MoS_2 phototransistor with a responsivity of 7.5 mA/W, which is higher than that of graphene [15]. Lee et al. investigated the layer-dependent photoresponse properties [16]. By improved mobility, contact quality, and positioning technique, a high responsivity of 880 A/W from an exfoliated monolayer MoS_2 was achieved by Andras Kis et al [17]. But the response speeds of above reported MoS_2 PDs are very slow, usually around few seconds, which limited the practical applications of MoS_2-based PDs. To further improve the response speed, heterostructures have been employed to achieve faster response speed *via* separation of photo-excited carriers by the built-in electric field at the interface [18-21].

Herein, the synthesis of large-area multilayer MoS_2 film *via* a thermal decomposition method, and *in situ* fabrication MoS_2/Si heterojunction devices were demonstrated. The optoelectrical properties of the fabricated devices were investigated, which exhibit excellent photoresponse properties with fast response speed, high responsivity, high specific detectivity and broad response region from deep ultraviolet (UV) to the near-infrared (NIR). This research finding confirms that this proposed MoS_2/Si heterojunction structure is very promising for high performance optoelectronic devices.

The multilayer MoS_2 thin films were synthesized *via* a two-step thermal decomposition process [13, 22]. First, *n*-Si substrates (resistivity: 1-10 $\Omega\cdot cm^{-1}$), which had been precleaned with acetone, alcohol and deionized water in an ultrasonic bath for 30 min each in sequence, were treated with Ar-plasma for hydrophilic

enhancement for 10 min. Then, 0.25 g of $(NH_4)_2MoS_4$ (Sigma-Aldrich, purity of 99.99%) was dissolved in 20 mL of dimethylformamide (DMF) to form a 1.25 wt% solution, which was further spin-coated on the substrate at a speed of 500 rpm for 10 s and then 3000 rpm for 30 s. The produced thin films were baked on a hot plate at 100 °C for 3 min to remove the solvent. Then the $(NH_4)_2MoS_4$ films were formed. The $(NH_4)_2MoS_4$ films were further annealed at 500 °C by filling with an Ar/H_2 (80/20 sccm) gas mixture to a pressure of 1.1 Torr for 60 min and subsequently annealed at 800 °C in the presence of sulfur under an 80 sccm flow of Ar to a pressure of 525 Torr for 40 min to synthesize the MoS_2 layers.

The as-synthesized layered MoS_2 thin films were characterized by X-ray diffraction (XRD, X' Pert Pro, Panalytical, Netherlands), high-resolution transmission electron microscopy (HRTEM, JEM-2010, JEOL, Japan), X-ray photoelectron spectroscopy (XPS, ESCALAB 250, Thermo Fisher Scientific, USA) and Raman spectroscopy (LabRAM HR Evolution, Horiba, Japan). The thickness of the as-synthesized MoS_2 thin film was determined by atomic force microscope (AFM, Dimension Icon, Bruker, USA).

After the preparation of MoS_2 thin films on Si substrates, Au electrodes (50 nm) on the MoS_2 thin film were fabricated by thermal evaporation *via* a shadow mask. In addition, a Cu foil was connected to a cross section of the Si by high-purity silver conducting paint. The schematic illustration of a MoS_2/Si heterojunction device is shown in Fig. 2a.

Electrical and optoelectrical measurements were conducted at room temperature with a semiconductor characterization system (Keithley 4200-SCS, Tektronix, USA) with a system combining a monochromator, light sources, an oscilloscope (DPO2012B, Tektronix, USA), a waveform generator (SDG1032X, Siglent, China), and a digital SourceMeter (Keithley 2636B, Tektronix, USA). In this work, a laser diode of 780 nm and a xenon lamp were used as light sources in the measurements.

Fig. 1a illustrates the XRD patterns of the obtained MoS_2 films on Si substrate. A strong peak at $2\theta = 14.3°$ was observed, corresponding to (002) crystal planes of MoS_2, which is usually observed when the periodicity in *c*-axis (normal to the MoS_2 film plane) is present. Fig. 1b shows the HRTEM image and the corresponding selected area electron diffraction (SAED) pattern with [001] zone axis (inset) for the MoS_2 thin film, which reveal the hexagonal lattice structure with the lattice spacing of 0.27 nm assigned to the (100) and (010) planes. Raman spectroscopy was employed to explore the structural properties of the as-synthesized MoS_2 film *via* the energy difference between the E_{2g} and A_{1g} Raman modes, as shown in Fig. 1c. Two typical Raman active modes of hexagonal MoS_2 are observed: E_{2g} at 382.44 cm^{-1} and A_{1g} at 407.92 cm^{-1}. The frequency difference between the A_{1g} and E_{2g} Raman modes, reflecting the number of MoS_2 layers, is 24.98 cm^{-1}, indicating the synthesis of a multilayer MoS_2 film. The thickness of the MoS_2 film was 9.5 nm according to AFM measurement, as shown in Fig. 1d. XPS measurements were recorded to determine the components and binding energies of the MoS_2 thin film, as shown in Fig. 1e and f. The peaks at 229.3 and 232.5 eV are related to the Mo 3d5/2 and Mo 3d3/2 orbitals, respectively, and the S 2p3/2 and S 2p1/2 orbitals are observed at 162.3 and 163.5 eV, respectively. The atomic ratio of Mo/S was determined to be 1:2.06, which is very close to the stoichiometric ratio of MoS_2. The results are in good agreement with the reported values for MoS_2 [23].

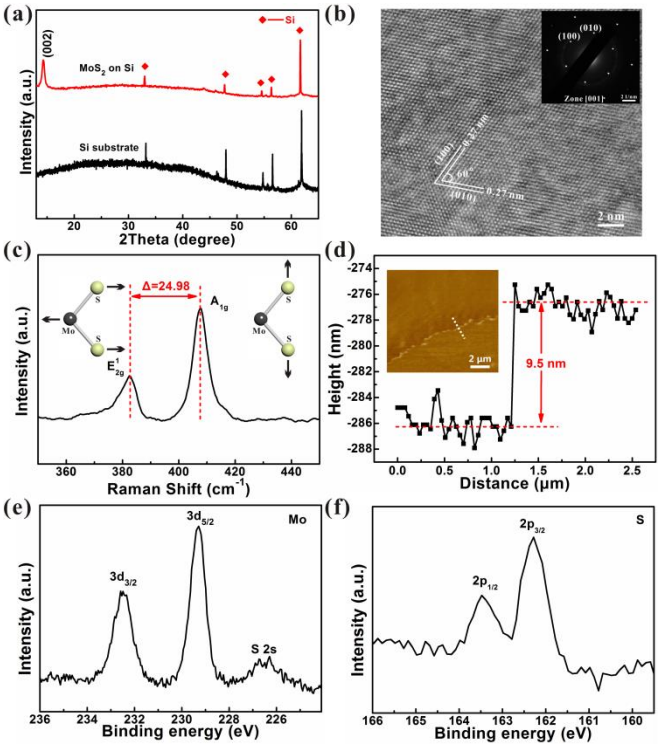

Fig. 1. (a) XRD patterns, (b) HRTEM and corresponding SAED pattern of MoS_2 thin film. (c) Raman spectrum, and (d) height profiles of a MoS_2 thin film. The XPS spectra show the binding energies of e) Mo and f) S of the MoS_2 thin film.

Fig. 2a depicts a schematic illustration of a MoS_2/Si heterojunction device. The current-voltage (*I-V*) curves of MoS_2/Si heterojunction device in the dark and under light illumination (780 nm, 72 mW/cm^2) were shown in Fig. 2b. From the curves, an obvious rectification characteristic with a rectification ratio of 13.1

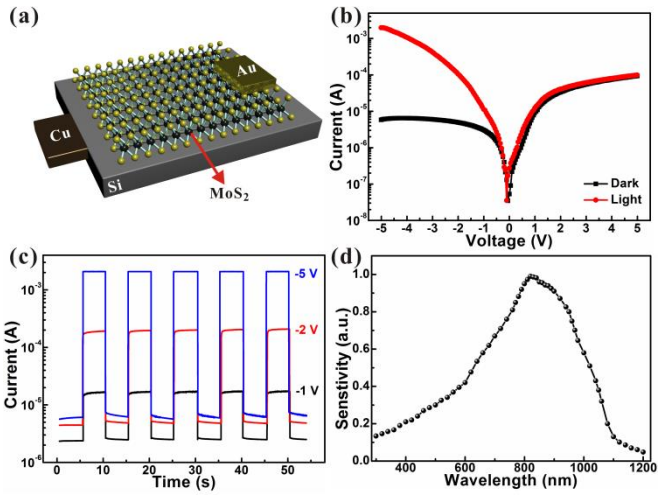

Fig. 2. (a) Schematic illustration of a MoS_2/Si heterojunction device. (b) I-V curves of MoS_2/Si heterojunction device in the dark and under light illumination (780 nm). (c) Photoresponse of the MoS_2/Si heterojunction under different bias voltages. (d) The sensitivities of the MoS_2/Si PD as a function of wavelength.

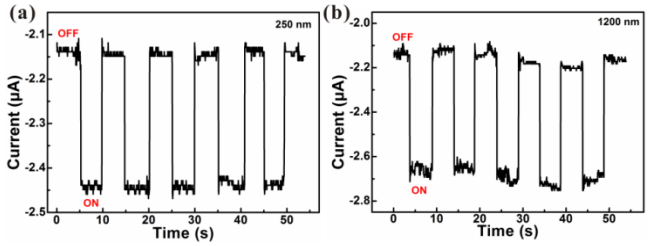

Fig. 3. Photoresponse of the MoS_2/Si heterojunction under incident light of (a) 250 nm and (b) 1200 nm at voltage bias of -1 V.

within ± 5 V can be obtained in the dark. And a remarkable increase of current of the device under reverse voltages can be found when the device was exposed to light illumination, leading to a high current on/off ratio (I_{light}/I_{dark}) over 3.15×10^2 at -5 V.

Hence, such MoS_2/Si heterojunction device can function as PDs. The photoresponse properties of this PD were investigated under different reverse voltage biases, as shown in Fig. 2c. The current reversibly switched between high and low conductance with high stability and repeatability when the light illumination (780 nm, 72 mW cm^{-2}) was turned on and off repetitively. The I_{light}/I_{dark} ratios were obtained to be 7.06, 43.4, and 347.2 under bias voltages of -1 V, -2 V, and -5 V, respectively. Fig. 2d shows the sensitivity of the MoS_2/Si PD as a function of wavelength. A clear photoresponse can be observed over a wide wavelength range from the UV to the NIR (300-1200 nm) with sensitivity peak around 820 nm. In addition, the photoresponse properties under deep ultraviolet (250 nm) and near-infrared (1200 nm) light illumination with intensity of 0.48 μW/cm^2 at voltage bias of -1 V were shown in Fig. 3. The remarkable response at UV and NIR region suggested that this MoS_2/Si heterojunction device is suitable for applications in broadband photodetectors from deep UV to NIR.

Furthermore, the light intensity-dependent photoresponse properties were investigated. The *I-V* curves of MoS_2/Si heterojunction PD under different light intensities from dark to 72

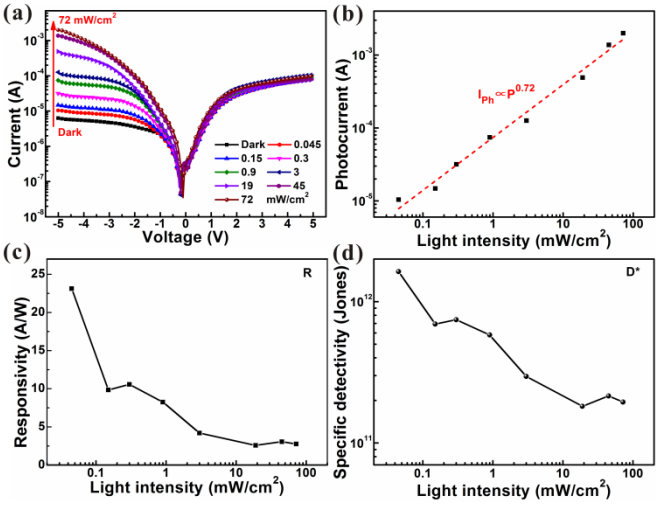

Fig. 4. (a) I-V curves of the MoS_2/Si heterojunction at varied light intensities (780 nm). (b) Logarithmic plot of the photocurrent *vs* light intensity. The curve is fitted well by the power law. Light intensity-dependent (c) responsivity and (d) specific detectivity at bias voltages of -5 V.

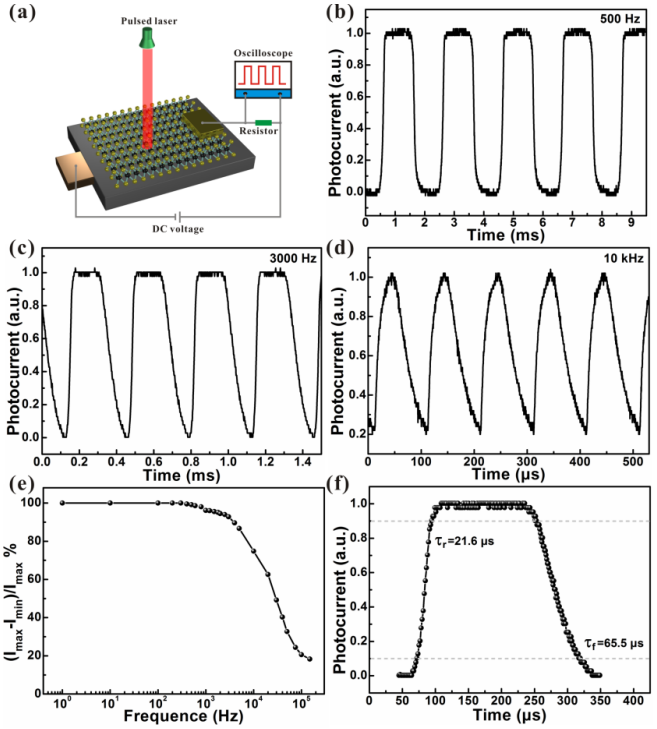

Fig. 5. (a) Schematic illustration of the measurement configuration for photoresponse detection. Photoresponse characteristics of the MoS_2/Si heterojunction to pulsed light irradiation at frequencies of (b) 500 Hz, (c) 3000 Hz and (d) 10 kHz. (e) The relative balance [$(I_{max}-I_{min})/I_{max}$] vs switching frequency. (f) Rising and falling edges for estimating rise time (τ_r) and the fall time (τ_f).

mW/cm^2 (780 nm) were shown in Fig. 4a. The photocurrent is highly dependent on the light intensity and it increases with increasing light intensity within reverse bias voltage measurement range. The dependence of photocurrent on the light intensity is plotted in Fig. 4b, and can be fitting by the power law ($I=AP^{\theta}$), where A is a constant for a given wavelength, and the exponent θdetermines the response of the photocurrent to light intensity. θ =0.72 can be obtained from the fitting curve. In addition, the responsivity (R) and specific detectivity (D*) are key parameters for a PD, which reflect the sensitivity of a PD to the incident light and the ability of a PD to detect a small optical signal, can be expressed by the following relations:[24]

$$R = \frac{I_P}{P_{opt}} \quad (1)$$

$$D^* = \frac{A^{1/2}R}{(2eI_d)^{1/2}} \quad (2)$$

where I_P, and P_{opt} are the photocurrent and the incident light intensity, respectively. A and I_d are the area and dark current of the PD. Based on equations above, R and D* under different light intensities were plotted in Fig. 4d. Both R and D* decrease with the increasing light intensity, and a responsivity of 23.1 A/W and specific detectivity of 1.63×10^{12} Jones (1 Jones =1 cm $Hz^{1/2}$ W^{-1}) can be obtained at light intensity of 45 μW/cm^2, which are much better than previous reported results [14, 19].

The response speed of a PD is directly related to its frequency response. It determines the ability of a PD to follow a fast-varying optical signal. To record an optical signal faithfully, a PD must have

a speed higher than the fastest temporal variations in the signal. In the time domain, the speed of a PD is characterized by the rise time (τ_r), and the fall time (τ_f). The risetime is defined as the time interval for the response to rise from 10 to 90% of its peak value, whereas the fall time is defined as the time interval for the response to decay from 90 to 10% of its peak value [25]. In our work, an oscilloscope was used to monitor the current variation of a resistor with time, and a laser diode of 780 nm controlled by a waveform generator was used as the light source, as shown in Fig. 5a. Fig. 5b-d show the photoresponse of the PD at incident light frequencies of 500 Hz, 3000 Hz and 10 kHz, respectively. The data have been normalized according to the highest photocurrent. The excellent stability and repeatability of MoS_2/Si PD were demonstrated. Furthermore, the relative balance $[(I_{max}-I_{min})/I_{max}]$ of the photocurrent over a wide frequency range up to 150 kHz were plotted in Fig. 5e. The relative balance can implying remain at 74.8% and 20.6% under a high frequency of 10 kHz and 100 kHz, respectively, implying that MoS_2/Si heterojunction PD is capable of monitoring ultrafast optical signals. Further analysis a single response cycle at 3000 Hz, a small τ_r of 21.6 μs and τ_f of 65.5 μs were obtained, which are superior to or close to previous results.

The high performances could be attributed to the high-quality heterojunction between MoS_2 and the Si obtained by *in situ* fabrication process. MoS_2 is more negative than that of Si due to the conduction band edge of MoS_2 is 250 meV [19]. The electrons would diffuse from Si into MoS_2 while holes should diffuse from MoS_2 into Si, thus a built-in electric field could be formed at the interface between MoS_2 and Si. Under light illumination with photon energy larger than the semiconductor bandgaps, the excitons will generate in both MoS_2 and Si at the interface, and then separated by the built-in electric field. When the heterojunction is applied with reverse bias, the electric field caused by reverse bias in depletion region is consistent with the build-in electric field, so the barrier height is enhanced. Meanwhile, the photo-generated minority carriers can pass through the interface easier owing to the strong external electric field, compared with that without bias. Therefore, photocurrent signals will be enhanced in this case, giving good photoresponse signal and fast transient response. Table 1 summarized the device performances of the MoS_2/Si PD and some reported MoS_2-based PDs.

Table 1. The summary of the device performances of MoS_2/Si PD and some reported MoS_2-based PDs.

Devices	I_{on}/I_{off}	R A/W	D* Jones	τ_r/τ_f μs	Ref.
MoS_2/Si	315	23.1	1.63×10^{12}	21.6/ 65.5	This work
MoS_2/Si	59.9	11.9	2.1×10^{10}	30.5/ 71.6	[19]
MoS_2 Schottky	~100	0.57	$\sim10^{10}$	70/ 110	[26]
MoS_2/Graphene	<1	0.032	/	$>10^6$/ 10^6	[14]
MoS_2/BP	/	22.3	3.1×10^{11}	15/70	[20]

In summary, MoS_2/Si heterojunction devices were *in situ* fabricated by synthesis of the large-scale multilayer MoS_2 thin films on Si substrates *via* a thermal decomposition method. The heterojunction devices exhibited pronounced photoresponse properties with high responsivity, high specific detectivity, fast response speeds and broad response region from deep ultraviolet to the near-infrared. The approach demonstrated here could be extended to the study of other 2D materials for high-performance PDs and may offer new possibilities toward practical optoelectronic applications.

Funding. National Natural Science Foundation of China (Nos. 61605174, 11504331), the China Postdoctoral Science Foundation (No. 2015M582194), Educational Department of Henan Province (No. 17A140012), Startup Research Fund of Zhengzhou University (1512317002), Research Grants Council of Hong Kong, China (Project Number: GRF 152109/16E PolyU B-Q52T).

References

1. M. Xu, T. Liang, M. Shi, and H. Chen, Chem. Rev. **113**, 3766 (2013).
2. X. Zhang, Z. C. Lai, C. L. Tan, and H. Zhang, Angew. Chem. Int. Ed. **55**, 8816 (2016).
3. S. Z. Butler, S. M. Hollen, L. Cao, Y. Cui, J. A. Gupta, H. R. Gutierrez, T. F. Heinz, S. S. Hong, J. Huang, and A. F. Ismach, ACS Nano **7**, 2898 (2013).
4. X. Song, J. Hu, and H. Zeng, J. Mater. Chem. C **1**, 2952 (2013).
5. K. F. Mak, C. Lee, J. Hone, J. Shan, and T. F. Heinz, Phys. Rev. Lett. **105**, 136805 (2010).
6. B. Radisavljevic, A. Radenovic, J. Brivio, V. Giacometti, and A. Kis, Nat. Nanotechnol. **6**, 147 (2011).
7. J. C. Shaw, H. Zhou, Y. Chen, N. O. Weiss, Y. Liu, Y. Huang, and X. Duan, Nano Research **7**, 511 (2015).
8. C. Ahn, J. Lee, H. U. Kim, H. Bark, M. Jeon, G. H. Ryu, Z. Lee, G. Y. Yeom, K. Kim, J. Jung, Y. Kim, C. Lee, and T. Kim, Adv. Mater. **27**, 5223 (2015).
9. S. Kim, A. Konar, W.-S. Hwang, J. H. Lee, J. Lee, J. Yang, C. Jung, H. Kim, J.-B. Yoo, J.-Y. Choi, Y. W. Jin, S. Y. Lee, D. Jena, W. Choi, and K. Kim, Nat. Commun. **3**, 1011 (2012).
10. B. Radisavljevic, M. B. Whitwick, and A. Kis, ACS Nano **5**, 9934 (2011).
11. C.-J. Shih, Q. H. Wang, Y. Son, Z. Jin, D. Blankschtein, and M. S. Strano, ACS Nano **8**, 5790 (2014).
12. Y. Xue, Y. Zhang, Y. Liu, H. Liu, J. Song, J. Sophia, J. Liu, Z. Xu, Q. Xu, Z. Wang, J. Zheng, Y. Liu, S. Li, and Q. Bao, ACS Nano **10**, 573 (2016).
13. Y. R. Lim, W. Song, J. K. Han, Y. B. Lee, S. J. Kim, S. Myung, S. S. Lee, K. S. An, C. J. Choi, and J. Lim, Adv. Mater. **28**, 5025 (2016).
14. C. Chen, Z. Feng, Y. Feng, Y. Yue, C. Qin, D. Zhang, and W. Feng, ACS Appl. Mater. Interfaces **8**, 19004 (2016).
15. Z. Yin, H. Li, H. Li, L. Jiang, Y. Shi, Y. Sun, G. Lu, Q. Zhang, X. Chen, and H. Zhang, ACS Nano **6**, 74 (2011).
16. H. S. Lee, S. W. Min, Y. G. Chang, M. K. Park, T. Nam, H. Kim, J. H. Kim, S. Ryu, and S. Im, Nano Lett. **12**, 3695 (2012).
17. O. Lopez-Sanchez, D. Lembke, M. Kayci, A. Radenovic, and A. Kis, Nat. Nanotechnol. **8**, 497 (2013).
18. Y. Zhang, Y. Yu, X. Wang, G. Tong, L. Mi, Z. Zhu, X. Geng, and Y. Jiang, J. Mater. Chem. C **5**, 140 (2017).
19. Y. Zhang, Y. Yu, L. Mi, H. Wang, Z. Zhu, Q. Wu, Y. Zhang, and Y. Jiang, Small **12**, 1062 (2016).
20. L. Ye, H. Li, Z. Chen, and J. Xu, ACS Photonics **3**, 692 (2016).
21. L. Z. Hao, W. Gao, Y. J. Liu, Y. M. Liu, Z. D. Han, Q. Z. Xue, and J. Zhu, Phys. Chem. Chem. Phys. **18**, 1131 (2015).
22. Y. H. Lee, X. Q. Zhang, W. Zhang, M. T. Chang, C. T. Lin, K. D. Chang, Y. C. Yu, J. T. Wang, C. S. Chang, L. J. Li, and T. W. Lin, Adv. Mater. **24**, 2320 (2012).
23. K. K. Liu, W. Zhang, Y. H. Lee, Y. C. Lin, M. T. Chang, C. Y. Su, C. S. Chang, H. Li, Y. Shi, H. Zhang, C. S. Lai, and L. J. Li, Nano Lett. **12**, 1538 (2012).
24. D. Wu, Y. Jiang, Y. G. Zhang, J. W. Li, Y. Q. Yu, Y. P. Zhang, Z. F. Zhu, L. Wang, C. Y. Wu, L. B. Luo, and J. S. Jie, J. Mater. Chem. **22**, 6206 (2012).
25. D. Wu, Y. Jiang, S. Y. Li, F. Z. Li, J. W. Li, X. Z. Lan, Y. G. Zhang, C. Y. Wu, L. B. Luo, and J. S. Jie, Nanotechnology **22**, 405201 (2011).
26. D.-S. Tsai, K.-K. Liu, D.-H. Lien, M.-L. Tsai, C.-F. Kang, C.-A. Lin, L.-J. Li, and J.-H. He, ACS Nano **7**, 3905 (2013).